EARTHQUAKE ENGINEERING AND STRUCTURAL DYNAMICS
Earthquake Engng Struct. Dyn. 2005; **34**:1129–1147
Published online 29 April 2005 in Wiley InterScience (www.interscience.wiley.com). DOI: 10.1002/eqe.471

Time-domain response of linear hysteretic systems to deterministic and random excitations

G. Muscolino[1,*,†], A. Palmeri[1] and F. Ricciardelli[2]

[1]*Department of Civil Engineering, University of Messina, Vill. Sant'Agata, 98166 Messina, Italy*
[2]*Department of Mechanics and Materials, University of Reggio Calabria, Via Graziella, Feo di Vito, 89060 Reggio Calabria, Italy*

SUMMARY

The causal and physically realizable Biot hysteretic model proves to be the simplest linear model able to describe the nearly rate-independent behaviour of engineering materials. In this paper, the performance of the Biot hysteretic model is analysed and compared with those of the ideal and causal hysteretic models. The Laguerre polynomial approximation (LPA) method, recently proposed for the time-domain analysis of linear viscoelastic systems, is then summarized and applied to the prediction of the dynamic response of linear hysteretic systems to deterministic and random excitations. The parameters of the LPA model generally need to be computed through numerical integrals; however, when this model is used to approximate the Biot hysteretic model, closed-form expressions can be found. Effective step-by-step procedures are also provided in the paper, which prove to be accurate also for high levels of damping. Finally, the method is applied to the dynamic analysis of a highway embankment excited by deterministic and random ground motions. The results show that in some cases the inaccuracy associated with the use of an equivalent viscous damping model is too large. Copyright © 2005 John Wiley & Sons, Ltd.

KEY WORDS: linear hysteretic damping; Biot model; Laguerre polynomial approximation; seismic analysis; random vibration; earth structures

1. INTRODUCTION

Energy is dissipated in vibrating systems through internal mechanisms, such as friction, phase-transformations, plasticity, viscosity and viscoelasticity, which are often impossible to perfectly identify and mathematically describe. Hence, a number of simple, macroscopic models are available in the literature for material damping, which for many engineering applications bring a quite satisfactory accuracy in the prediction of the system response.

*Correspondence to: G. Muscolino, Department of Civil Engineering, University of Messina, Vill. Sant'Agata, 98166 Messina, Italy.
†E-mail: muscolin@ingegneria.unime.it

Received 26 June 2003
Revised 5 August 2004
Accepted 7 January 2005

Owing to its simplicity, the most widely used among linear models is the Kelvin–Voigt (KV) model, in which the damping is purely viscous and the energy lost in a harmonic cycle linearly increases with frequency. However, experimental analyses showed that the dissipation of a number of engineering materials, e.g. soils, asphalt, polymers and rubber, is nearly frequency-independent. When, in addition, the dissipation is proportional to the square of the vibration amplitude, as occurs for small amplitude oscillations, the material is said to have a 'linear hysteretic' behaviour, and alternative models have been proposed for its mathematical description.

Both real- and complex-valued representations have been considered [1–4] in formulating ideal hysteretic (IH) models, which provide a damping force proportional to the displacement but in phase with the velocity, therefore bringing a frequency-independent dissipation. Such ideal definition, however, can be rigorously used only in the frequency domain, since in the time domain it brings a non-causality flaw [5], i.e. response prior to excitation. Although there is no physically realizable linear model in which the dissipation is strictly independent of frequency, the problem arises of formulating a consistent time-domain model for materials having an almost constant dissipation in a specified interval of frequencies [6].

Given the theoretical and practical relevance of the IH damping, a number of papers has been published in the last two decades about this topic. Gaul, Bohlen and Kempfle [7] investigated the deviations from the initial conditions due to the non-causality. Milne [8] derived the closed-form expression of the impulse-response function of a linear SDoF oscillator with IH damping. Inaudi and Kelly [9] presented a consistent time-domain representation for the IH damping, based on the Hilbert transform operator. The same idea can be found in the papers of Chen and You [10, 11], in which alternative numerical procedures are provided to solve the integrodifferential equations of motion of IH systems. Inaudi and Makris showed that the use of analytical (complex-valued) signals allows these equations to be turned into differential equations with complex-valued coefficients and analytical input [12, 13].

The above studies, however, do not overcome the non-causality flaw of the IH damping. This issue has been addressed in two companion papers by Makris [14, 15]. In the first, the relation between analyticity of dynamic stiffness and causality of the corresponding time-domain response is extended to generalized functions; in the second, a causal hysteretic (CH) model is constructed, using this formulation. A singularity at the static limit, unfortunately, makes the CH model pathological.

In Reference [15], furthermore, Makris demonstrated that the CH model can be viewed as the high-frequency limit of the long-neglected Biot hysteretic (BH) model. The latter is a linear viscoelastic model, which is able to approximate the hysteretic behaviour without the non-causality flaw. It was proposed by Biot [16] almost fifty years ago, just as a particular case in a paper on the thermodynamics of linear irreversible processes. Four years later, Caughey [5] elucidated that the BH model can be formally represented as an elastic spring in parallel with an infinite number of Maxwell elements, and gave some exact solutions. Recently, Makris and Zhang [17] showed how the dynamic analysis of linear MDoF earth structures can be rigorously conducted by modelling the dissipation through the BH model; in the paper, the use of the Prony approximation is proposed in order to compute the seismic response in the time domain, so avoiding the solution of the integrodifferential equations of motion associated with the BH model. Finally, Spanos and Tsavachidis [18] proposed two different approaches to minimize the computational burden of time-domain analyses of structures featuring a BH damping, with applications to the seismic response of SDoF oscillators with cubic stiffness:

the first uses a recursive algorithm to compute the hysteretic force, while the second uses digital filters designed in the frequency domain.

As opposed to the large number of papers dealing with linear hysteretic systems under deterministic excitations, only in a few works the response to random excitations is coped with. In particular, this topic has been recently addressed in two papers by Spanos and his co-workers. In Reference [19], it is elucidated that the state–space formulation for the IH models is unstable in the bound input–bound output sense; as a consequence, this approach cannot be appropriately used for random vibrations. In Reference [18], the method of statistical linearization is employed to estimate the variance of the stationary response of SDoF oscillators with cubic stiffness and BH damping to white noise. However, to the best of our knowledge, no approaches are available in the literature to evaluate the non-stationary response statistics of linear hysteretic structures under random excitations.

In this paper, the Laguerre polynomial approximation (LPA) method, recently proposed for the time-domain analysis of viscoelastic systems, is particularized to the case of linear hysteretic damping, described through the BH model. After some preliminary concepts, and a discussion on the IH, CH and BH models, the main features of the LPA method are outlined. The method, originally formulated for SDoF oscillators under deterministic excitations [20], proved effective also in the case of MDoF systems [21], and for stationary and non-stationary, white and non-white random excitations [22]. Numerical procedures of solution are given in the cases of deterministic and random excitations. Contrary to other approximations available in the literature, closed-form expressions are also provided for the LPA parameters when this is applied to the BH model. The accuracy of the proposed approach is investigated in depth. Finally, the procedure is applied to a highway embankment, in order to demonstrate that the LPA model enables the prediction of the response of MDoF structural systems under deterministic and random ground motions.

2. PRELIMINARY CONCEPTS

For a SDoF oscillator, made of a mass m grounded through a linear link, the equation of motion in the time domain is:

$$m\ddot{x}(t) + k_0 x(t) + r(t) = f(t) \tag{1}$$

where $x(t)$ is the mass displacement, $f(t)$ is the exciting force, k_0 is the equilibrium modulus, corresponding to the static stiffness, and $r(t)$ is the dissipative force, i.e. the force exerted by the linear link, not including the elastic portion. The solution of Equation (1) in the frequency domain is:

$$\mathscr{F}\langle x(t)\rangle = \frac{1}{m} H(\omega)\mathscr{F}\langle f(t)\rangle; \quad H(\omega) = \left[\frac{1}{m}K(\omega) - \omega^2\right]^{-1}$$

where $\mathscr{F}\langle\cdot\rangle$ stands for the Fourier transforms operator, $H(\omega)$ is the complex-valued Frequency Response Function (FRF), and $K(\omega)$ is the complex-valued dynamic stiffness of the linear link, defined as:

$$K(\omega) = K_1(\omega) + \mathrm{j}K_2(\omega) = k_0 + \frac{\mathscr{F}\langle r(t)\rangle}{\mathscr{F}\langle x(t)\rangle}$$

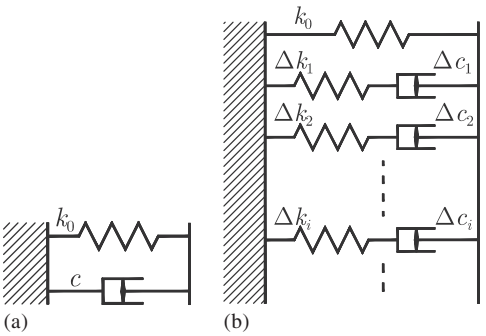

Figure 1. Schematic representations of: (a) the Kelvin–Voigt model; and (b) the viscoelastic Biot hysteretic model.

where $K_1(\omega)$ and $K_2(\omega)$ are the real-valued storage and loss moduli, that are even and odd functions of frequency, respectively. It can be shown that the loss modulus fully accounts for the dissipation properties; when $x(t)$ is the steady state response to a harmonic excitation, in fact, the energy dissipated per cycle, W_d, is proportional to the loss modulus and to the square of the vibration amplitude $\bar{x}$:

$$W_\mathrm{d} = \oint r(t)\,\mathrm{d}x(t) = \pi \bar{x}^2 K_2(\bar{\omega}) \tag{2}$$

in which $\bar{\omega}$ is the circular frequency of the excitation.

A number of mathematical models can be used to describe the constitutive law of linear dynamic systems, the most common being the Kelvin–Voigt (KV) model (Figure 1(a)), consisting of an elastic spring $k_0 \equiv K_1(0)$ in parallel with a viscous dashpot c. The dissipative force $r(t)$ and the dynamic stiffness $K(\omega)$ of the KV model particularize as:

$$r_\mathrm{KV}(t) = c\dot{x}(t); \quad K_\mathrm{KV}(\omega) = k_0 + \mathrm{j}c\omega \tag{3}$$

in which the subscripts denote the particular model of the linear link. Equations (2) and (3) show that for the KV model the energy dissipated per harmonic cycle is proportional to the vibration frequency:

$$W_{\mathrm{d,KV}} = \pi \bar{x}^2 c \bar{\omega}$$

Even though simplistic, the KV model is widely used in structural dynamics, since this one is the only linear model for which the structural response at a given time instant does not depend on the previous history of the response itself. In fact, substitution of the first of Equations (3) into Equation (1) brings a second-order differential equation, easy to solve with standard techniques:

$$\ddot{x}(t) + 2\zeta_\mathrm{V}\omega_0\dot{x}(t) + \omega_0^2 x(t) = \frac{1}{m} f(t) \tag{4}$$

where $\omega_0 = \sqrt{k_0/m}$ and $\zeta_\mathrm{V} = c/(2m\omega_0)$ are the undamped natural circular frequency and viscous damping ratio, respectively, while $T_0 = 2\pi/\omega_0$ is the undamped natural period.

3. LINEAR HYSTERETIC MODELS

Owing to its simplicity, the KV model is the most commonly used for linear dynamic systems. However, its dissipation properties do not correspond to the observed behaviour of a number of engineering materials, that experimental studies have indicated as nearly hysteretic in the linear range. In this section, then, the main features of three different linear hysteretic models available in the literature will be briefly summarized.

3.1. Ideal (non-causal) hysteretic model

Equation (2) suggests that for an ideal hysteretic (IH) model the loss modulus needs to be constant with frequency and, consistently, the dynamic stiffness is written as:

$$K_{\mathrm{IH}}(\omega) = k_0[1 + \mathrm{j}\eta_{\mathrm{H}} \operatorname{sign}(\omega)] \tag{5}$$

where η_{H} is the frequency-independent loss factor (i.e. the ratio of the constant loss and storage moduli), and the signum function is added to make the loss modulus an odd function of frequency. The energy dissipated per cycle, then, is independent of frequency:

$$W_{\mathrm{d,IH}} = \pi \bar{x}^2 \eta_{\mathrm{H}} k_0 \tag{6}$$

The consistent time-domain representation of the dissipative force for the IH model is [9]:

$$r_{\mathrm{IH}}(t) = \eta_{\mathrm{H}} k_0 \mathscr{H}\langle x(t)\rangle; \quad \mathscr{H}\langle x(t)\rangle = -\frac{1}{\pi}\int_{-\infty}^{+\infty} \frac{x(s)}{t-s}\,\mathrm{d}s \tag{7}$$

where $\mathscr{H}\langle\cdot\rangle$ stands for the Hilbert transform operator.

Substitution of Equations (7) into Equation (1) allows the following integrodifferential equation of motion to be written:

$$m\ddot{x}(t) + k_0[x(t) + \eta_{\mathrm{H}} \mathscr{H}\langle x(t)\rangle] = f(t) \tag{8}$$

Unfortunately, because of the anticipatory property of the Hilbert transform, Equation (8) is non-causal, i.e. the response $x(t)$ precedes the application of the input $f(t)$.

3.2. Causal hysteretic model

By virtue of the Kramers–Kroning relations, storage and loss moduli of linear dynamic systems cannot be defined independently, as for the system to be causal the dynamic stiffness needs to be an analytical function of frequency [14]. That is:

$$K_1(\omega) = k_0 - \mathscr{H}\langle K_2(\omega)\rangle; \quad K_2(\omega) = \mathscr{H}\langle K_1(\omega)\rangle \tag{9}$$

Equation (5) does not satisfy Equations (9); so, the IH model is non-causal. In order to circumvent this problem, Makris [15] formulated a causal hysteretic (CH) model, which has the same loss modulus as the IH model, but with a modified storage modulus that makes the model causal:

$$K_{\mathrm{CH}}(\omega) = k_0 \left[1 + \frac{2\eta_{\mathrm{H}}}{\pi} \ln\left|\frac{\omega}{\varepsilon}\right| + \mathrm{j}\eta_{\mathrm{H}} \operatorname{sign}(\omega)\right] \tag{10}$$

The energy dissipated in a steady-state harmonic cycle is still given by Equation (6), because the imaginary parts of Equations (5) and (10) coincide. However, for $\omega > \varepsilon$ the CH model is

stiffer than the IH model, since the storage modulus is increased by the logarithmic term in Equation (10).

It can be shown that the integrodifferential equation of motion for SDoF oscillators with CH damping, at rest for $t<0$, is:

$$m\ddot{x}(t)+k_0\left[x(t)-\frac{\eta_H}{\pi}\int_0^t\frac{x(s)}{t-s}\,\mathrm{d}s\right]=f(t) \tag{11}$$

It is worth noting that when the second of Equations (7) is introduced into Equation (8), the only difference with Equation (11) is given by the limits of integration in the convolution integral. In Equation (8) the convolution is extended from $-\infty$ to $+\infty$, while in Equation (11) it is bounded to the time interval $[0,t]$, which brings causality.

The flaw of the CH model is that it is not defined at the static limit [15], because of the negative singularity at $\omega=0$, which affects the dynamic stiffness of Equation (10). In addition, as a further symptom of a physical inconsistency, the storage modulus becomes negative for $\omega<\exp(-1.57/\eta_H)\varepsilon$. Then, even though the conceptual significance of the CH model is out of doubt, its applicability to practical situations is not unconditional.

3.3. Biot hysteretic model

In the previous subsections it has been shown that it is impossible to obtain a linear model which is causal and in which both loss and storage moduli are rate independent. The IH model, in fact, does not satisfy causality, while in the CH model the causality constraint requires the storage modulus to increase with frequency as the logarithm of $|\omega/\varepsilon|$ and, as a consequence, a singularity appears for $\omega\to 0$. A third possibility is the Biot hysteretic (BH) model, in which both loss and storage moduli vary with frequency, and which seems to be the simplest, causal and physically realizable linear model able to approximate the hysteretic damping [17].

The BH model can be viewed as a continuous representation of the discrete model depicted in Figure 1(b), made of a spring k_0 in parallel with a large number N of Maxwell elements [5]. The i-th one is made of an elastic spring Δk_i in series with a viscous dashpot $\Delta c_i=\Delta k_i t_i$, given by:

$$\Delta k_i=\frac{2\eta_H k_0}{(i-0.5)\pi};\quad t_i=\frac{i-0.5}{\varepsilon N}$$

where ε is a free parameter having the dimensions of a frequency. As $N\to\infty$, the dynamic stiffness becomes:

$$K_{BH}(\omega)=k_0\left\{1+\frac{2}{\pi}\eta_H\left[\ln\sqrt{1+\left(\frac{\omega}{\varepsilon}\right)^2}+\mathrm{j}\arctan\left(\frac{\omega}{\varepsilon}\right)\right]\right\} \tag{12}$$

From Equation (12), it follows that the ε parameter controls the rate of increase with ω of both storage and loss moduli. When $\varepsilon\ll|\omega|$ the dynamic stiffness of Equation (12) tends to the dynamic stiffness of Equation (10), i.e. the CH model is the high-frequency limit of the BH model [15]. Moreover, Equation (12) tells that the ε parameter cannot be too small, otherwise the real part of Equation (12) may became too large, so excessively increasing the

stiffness of the system under dynamic loads. On the other hand, the ε parameter cannot be too large. In fact, substitution of Equation (12) into Equation (2) allows:

$$W_{\mathrm{d,BH}} = 2\bar{x}^2 \eta_{\mathrm{H}} k_0 \arctan\left(\frac{\omega}{\varepsilon}\right) \tag{13}$$

and the comparison with Equation (6) suggests the ε parameter be chosen small enough, such that $\arctan(\omega/\varepsilon) \cong \pi/2$ in the frequency range of interest. Although a general rule cannot be defined, in many practical situations $\varepsilon = \omega_0/10$ seems to be a satisfactory choice [9, 17], implying that at resonance the loss modulus is more than 90% of the corresponding frequency-independent value, while the storage modulus is approximately 30% larger than its static limit. Higher values of ε bring a storage modulus closer to the static limit, but the dissipation is hysteretic only at the high frequencies. Conversely, lower values of ε make the BH model hysteretic also towards the low frequencies, but the system stiffness tends to be overestimated.

The equation of motion of a linear SDoF oscillator with BH damping can be written in the following integrodifferential form (e.g. [17, 18]):

$$m\ddot{x}(t) + k_0 \left\{ x(t) - \frac{2\eta_{\mathrm{H}}}{\pi} \int_0^t \mathrm{Ei}[-\varepsilon(t-s)]\,\dot{x}(s)\,\mathrm{d}s \right\} = f(t) \tag{14}$$

where the main difficulty in integrating is related to the time-dependent convolution integral:

$$q_\varepsilon(t) = \int_0^t \mathrm{Ei}[-\varepsilon(t-s)]\dot{x}(s)\,\mathrm{d}s; \quad \mathrm{Ei}(x) = \int_x^\infty \frac{\mathrm{e}^{-s}}{s}\,\mathrm{d}s \tag{15}$$

$\mathrm{Ei}(\cdot)$ being the exponential integral function.

4. LAGUERRE POLYNOMIAL APPROXIMATION FOR THE BIOT HYSTERETIC MODEL

4.1. Proposed model

In the previous section it has been emphasized that the BH model is not affected by physical inconsistencies, and can be viewed as the simplest model to be used in time-domain analyses of linear hysteretic systems. However, the use of the BH model requires the solution of convolution integrals, with a high computational demand. In this section, as an alternative to other approaches available in the literature, the Laguerre polynomial approximation (LPA) model, recently formulated by Palmeri *et al.* [20] for linear viscoelastic systems, will be proposed for the approximated solution of Equation (14). The method allows turning the integrodifferential equation of motion into a set of differential equations, so reducing the computational effort.

Initially, let us rewrite Equation (14) in a state–space form:

$$\begin{cases} \dot{x}_1(t) = x_2(t) \\ \dot{x}_2(t) = -\omega_0^2 x_1(t) + \alpha q_\varepsilon(t) - \dfrac{1}{m} f(t) \end{cases} \tag{16}$$

where $x_1(t)=x(t)$ and $x_2(t)=\dot{x}(t)$ are the classical state variables, the additional coordinate $q_\varepsilon(t)$ is given through Equations (15), and $\alpha=2\omega_0^2\eta_H/\pi$.

The main idea underlying the proposed method is to approximate the term $\alpha q_\varepsilon(t)$ as the linear combination of N_λ additional internal variables (AIVs), introduced to account for the system response in the time interval $[0,t]$:

$$\alpha q_\varepsilon(t)\cong\sum_{i=0}^{N_\lambda-1}a_i\lambda_i(t) \tag{17}$$

where the i-th Laguerre stiffness a_i can be computed as:

$$a_i=\alpha\left[\frac{1}{\tau_0}\int_0^{+\infty}\mathrm{Ei}(-\varepsilon t)\mathrm{L}_i\left(\frac{t}{\tau_0}\right)\mathrm{d}t\right]$$

$\mathrm{L}_i(\cdot)$ being the i-th Laguerre polynomial and τ_0 being an equivalent relaxation time, and where the time variation of the i-th Laguerre strain $\lambda_i(t)$ is governed by the first-order linear differential equation:

$$\dot{\lambda}_i(t)=x_2(t)-\frac{1}{\tau_0}\sum_{k=0}^{i}\lambda_k(t) \tag{18}$$

Equations (16), (17) and (18), then, are a set of linear differential equations of order $N_\lambda+2$. In a more compact form, one can write:

$$\begin{cases}\dot{\mathbf{x}}(t)=\mathbf{A}_\mathrm{x}\mathbf{x}(t)+\mathbf{A}_{\mathrm{x}\lambda}\boldsymbol{\lambda}(t)+\dfrac{1}{m}\mathbf{b}_\mathrm{x}f(t)\\ \dot{\boldsymbol{\lambda}}(t)=\mathbf{A}_\lambda\boldsymbol{\lambda}(t)+\mathbf{A}_{\lambda\mathrm{x}}\mathbf{x}(t)\end{cases} \tag{19}$$

in which:

$$\mathbf{A}_\mathrm{x}=\begin{bmatrix}0 & 1\\ -\omega_0^2 & 0\end{bmatrix};\quad \mathbf{A}_{\mathrm{x}\lambda}=-\begin{bmatrix}0 & 0 & \cdots & 0\\ a_0 & a_1 & \cdots & a_{N_\lambda-1}\end{bmatrix};\quad \mathbf{b}_\mathrm{x}=\begin{bmatrix}0\\ 1\end{bmatrix}$$

$$\mathbf{A}_{\lambda\mathrm{x}}=\begin{bmatrix}0 & 1\\ 0 & 1\\ \vdots & \vdots\\ 0 & 1\end{bmatrix};\quad \mathbf{A}_\lambda=-\tau_0^{-1}\begin{bmatrix}1 & 0 & \cdots & 0\\ 1 & 1 & \cdots & 0\\ \vdots & \vdots & \ddots & 0\\ 1 & 1 & \cdots & 1\end{bmatrix}$$

In the enlarged state space, Equations (19) take the expression:

$$\dot{\mathbf{z}}(t)=\mathbf{A}\mathbf{z}(t)+\frac{1}{m}\mathbf{b}f(t) \tag{20}$$

where $\mathbf{z}(t)=[\mathbf{x}(t)^\mathrm{T}|\boldsymbol{\lambda}(t)^\mathrm{T}]^\mathrm{T}$ is the complete state vector of order $N_\lambda+2$, and the dynamic matrix and the influence vector are:

$$\mathbf{A}=\left[\begin{array}{c|c}\mathbf{A}_\mathrm{x} & \mathbf{A}_{\mathrm{x}\lambda}\\ \hline \mathbf{A}_{\lambda\mathrm{x}} & \mathbf{A}_\lambda\end{array}\right];\quad \mathbf{b}=\left[\begin{array}{c}\mathbf{b}_\mathrm{x}\\ \hline \mathbf{O}_{N_\lambda\times 1}\end{array}\right]$$

$\mathbf{O}_{i\times k}$ being a null block of i rows and k columns.

4.2. Response to deterministic loading

When the excitation is deterministic, the solution of Equation (20) can be written as [20]:

$$\mathbf{z}(t) = \boldsymbol{\Theta}(t)\mathbf{z}_0 + \frac{1}{m}\int_0^t \boldsymbol{\Theta}(t-\tau)\mathbf{b}f(\tau)\,\mathrm{d}\tau$$

where $\mathbf{z}_0 = \mathbf{z}(0)$ accounts for the initial conditions, and the transition matrix $\boldsymbol{\Theta}(t)$ is:

$$\boldsymbol{\Theta}(t) = \exp\langle \mathbf{A}t \rangle$$

with $\exp\langle\cdot\rangle$ standing for the exponential matrix of the square matrix into angle brackets. Once the transition matrix is computed for the selected sampling time Δt, an incremental solution of Equation (20) can be obtained through the following, unconditionally stable, step-by-step procedure [23]:

$$\mathbf{z}(t_{n+1}) = \boldsymbol{\Theta}(\Delta t)\mathbf{z}(t_n) + \boldsymbol{\gamma}_0(\Delta t)f(t_n) + \boldsymbol{\gamma}_1(\Delta t)f(t_{n+1}) \tag{21}$$

in which $t_i = i\Delta t$, and the linear-load vectors are:

$$\begin{cases} \boldsymbol{\gamma}_0(\Delta t) = \dfrac{1}{m}\left[\boldsymbol{\Theta}(\Delta t) - \dfrac{\mathbf{L}(\Delta t)}{\Delta t}\right]\mathbf{A}^{-1}\mathbf{b} \\ \boldsymbol{\gamma}_1(\Delta t) = \dfrac{1}{m}\left[\dfrac{\mathbf{L}(\Delta t)}{\Delta t} - \mathbf{I}_{N_\lambda+2}\right]\mathbf{A}^{-1}\mathbf{b} \end{cases} ; \quad \mathbf{L}(\Delta t) = [\boldsymbol{\Theta}(\Delta t) - \mathbf{I}_{N_\lambda+2}]\mathbf{A}^{-1}$$

4.3. Response to random noise

In a number of engineering situations dynamic loads cannot be described in a deterministic fashion. For instance, natural actions on structures, such as earthquakes, wind and waves are often modelled as stationary or non-stationary random processes. The linearity of the LPA method makes its extension to stochastic loading quite straightforward, and in the following a numerical procedure to compute the second-order statistics of the response for a SDoF oscillator with linear hysteretic damping to non-stationary filtered white noise will be derived. In the case of a time-invariant linear filter, the governing equations are:

$$\begin{cases} \dot{\mathbf{x}}(t) = \mathbf{A}_\mathrm{x}\mathbf{x}(t) + \mathbf{A}_{\mathrm{x}\lambda}\boldsymbol{\lambda}(t) + \mathbf{A}_{\mathrm{xf}}\mathbf{x}_\mathrm{f}(t) \\ \dot{\boldsymbol{\lambda}}(t) = \mathbf{A}_\lambda\boldsymbol{\lambda}(t) + \mathbf{A}_{\lambda\mathrm{x}}\mathbf{x}(t) \\ \dot{\mathbf{x}}_\mathrm{f}(t) = \mathbf{A}_\mathrm{f}\mathbf{x}_\mathrm{f}(t) + \mathbf{b}_\mathrm{f}\varphi(t)w(t) \end{cases} \tag{22}$$

where $\mathbf{x}_\mathrm{f}(t)$ is the array listing the N_f state variables of the filter, $\mathbf{A}_\mathrm{f}$, $\mathbf{b}_\mathrm{f}$ and $\mathbf{A}_{\mathrm{xf}}$ collect the parameters of the filter, $\varphi(t)$ is a deterministic amplitude-modulating function, and $w(t)$ is a sample of a stationary, zero-mean, Gaussian white noise, with power spectral density S_W. As an example, when the Kanai–Tajimi filter is used in the seismic analyses of structures, the ground acceleration is modelled as the absolute acceleration of a linear SDoF oscillator driven by white noise, with properly chosen values of natural frequency and damping ratio.

In the state space, enlarged to include also the state variables of the filter, Equations (22) become:

$$\dot{\bar{\mathbf{z}}}(t) = \bar{\mathbf{A}}\bar{\mathbf{z}}(t) + \bar{\mathbf{b}}\varphi(t)w(t)$$

where $\bar{\mathbf{z}}(t) = [x(t)^{\mathrm{T}} | \boldsymbol{\lambda}(t)^{\mathrm{T}} | \mathbf{x}_{\mathrm{f}}(t)^{\mathrm{T}}]^{\mathrm{T}}$ is the complete state vector of order $N_\lambda + N_{\mathrm{f}} + 2$, and the dynamic matrix and the influence vector are:

$$\bar{\mathbf{A}} = \left[\begin{array}{c|c|c} \mathbf{A}_{\mathrm{x}} & \mathbf{A}_{\mathrm{x}\lambda} & \mathbf{A}_{\mathrm{xf}} \\ \hline \mathbf{A}_{\lambda\mathrm{x}} & \mathbf{A}_{\lambda} & \mathbf{O}_{N_\lambda \times N_{\mathrm{f}}} \\ \hline \mathbf{O}_{N_{\mathrm{f}} \times 2} & \mathbf{O}_{N_{\mathrm{f}} \times N_\lambda} & \mathbf{A}_{\mathrm{f}} \end{array}\right]; \quad \bar{\mathbf{b}} = \left[\begin{array}{c} \mathbf{O}_{2\times 1} \\ \hline \mathbf{O}_{N_\lambda \times 1} \\ \hline \mathbf{b}_{\mathrm{f}} \end{array}\right]$$

The second-order statistics of the oscillator-filter state variables are listed in the covariance vector $\boldsymbol{\sigma}_{\bar{z}}(t) = \mathrm{E}\langle \bar{\mathbf{z}}(t) \otimes \bar{\mathbf{z}}(t) \rangle$, where $\mathrm{E}\langle\cdot\rangle$ and $\otimes$ stand for the expectation operator and for the Kronecker product [22, 23], respectively. The equation governing the time variation of the covariance vector is:

$$\dot{\boldsymbol{\sigma}}_{\bar{z}}(t) = \bar{\mathbf{A}}_2 \boldsymbol{\sigma}_{\bar{z}}(t) + 2\pi S_W \bar{\mathbf{b}}_2 \varphi^2(t) \tag{23}$$

in which the forcing term is the square of the amplitude-modulating function, and

$$\bar{\mathbf{A}}_2 = \bar{\mathbf{A}} \otimes \mathbf{I}_{N_\lambda + N_{\mathrm{f}} + 2} + \mathbf{I}_{N_\lambda + N_{\mathrm{f}} + 2} \otimes \bar{\mathbf{A}}; \quad \bar{\mathbf{b}}_2 = \bar{\mathbf{b}} \otimes \bar{\mathbf{b}}$$

Finally, an incremental solution can be found through the following unconditionally stable, step-by-step procedure:

$$\boldsymbol{\sigma}_{\bar{z}}(t_{n+1}) = \bar{\boldsymbol{\Theta}}_2(\Delta t) \boldsymbol{\sigma}_{\bar{z}}(t_n) + \pi S_W \bar{\mathbf{L}}_2(\Delta t) \bar{\mathbf{b}}_2 [\varphi^2(t_n) + \varphi^2(t_{n+1})] \tag{24}$$

where the transition matrix and the constant-load matrix are to be computed as:

$$\begin{cases} \bar{\boldsymbol{\Theta}}_2(\Delta t) = \bar{\boldsymbol{\Theta}}(\Delta t) \otimes \bar{\boldsymbol{\Theta}}(\Delta t) \\ \bar{\mathbf{L}}_2(\Delta t) = [\bar{\boldsymbol{\Theta}}_2(\Delta t) - \mathbf{I}_{(N_\lambda + N_{\mathrm{f}} + 2)^2}] \bar{\mathbf{A}}_2^{-1} \end{cases}; \quad \bar{\boldsymbol{\Theta}}(\Delta t) = \exp\langle \bar{\mathbf{A}} \Delta t \rangle$$

It is worth noting that the incremental solutions of Equations (21) and (24) have similar forms, being of similar form to Equations (20) and (23). In the deterministic loading case, however, it is assumed that the excitation varies linearly in each time step, which does not introduce further approximations in the solution when recorded ground motions are considered. In the stochastic loading case, on the other hand, it is assumed that the forcing term is constant in each time step, and the latter assumption is justified through the fact that realistic amplitude modulating functions $\varphi(t)$ are smoother than any possible recorded or generated loading time history.

4.4. *Calibration of model parameters*

As shown by Palmeri *et al.* [20], the accuracy of the LPA method in approximating a generic viscoelastic system depends only on the equivalent relaxation time τ_0 and on the number N_λ of AIVs. In principle, τ_0 can be arbitrarily chosen, as the orthonormal properties of the Laguerre polynomials allow an accurate approximation of any relaxation function, provided N_λ is sufficiently large. In the case of the BH model, however, two choices are straightforward, which are associated with the simplest closed-form expressions for the a_i coefficients. The first is:

$$\tau_0 = \frac{1}{\varepsilon} \quad \Rightarrow \quad a_i = \frac{\alpha}{i+1}$$

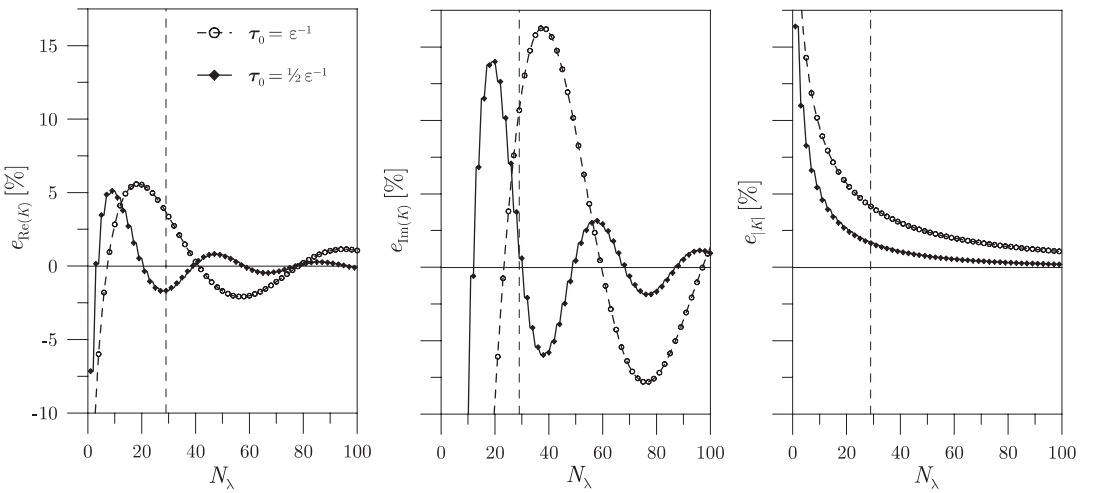

Figure 2. Percentage errors between the Biot hysteretic model and the Laguerre polynomial approximation for storage modulus $\mathrm{Re}(K)$, loss modulus $\mathrm{Im}(K)$, and absolute value of dynamic stiffness $|K|$ at resonance.

while the second is:

$$\tau_0 = \frac{1}{2\varepsilon} \quad \Rightarrow \quad a_i = \alpha \frac{1 + (-1)^i}{i + 1} \tag{25}$$

Even if in both cases the coefficients a_i decrease as $(i+1)^{-1}$, Equations (25), in which the odd ones are zero, allow a faster convergence, and then have to be preferred. This is shown in Figure 2, where the percentage errors in terms of storage modulus $e_{\mathrm{Re}(K)}$, loss modulus $e_{\mathrm{Im}(K)}$, and absolute value of the dynamic stiffness $e_{|K|}$ at resonance are depicted for $\eta_{\mathrm{H}} = 0.30$ and $\varepsilon = \omega_0/10$. The broken lines indicate $N_\lambda = 29$, corresponding to a negligible discrepancy in the loss modulus, this being the dominant term in the FRF at resonance.

In Figure 3 the dimensionless storage and loss moduli of the BH model for $\eta_{\mathrm{H}} = 0.30$ are compared with those of the corresponding LPA models with $N_\lambda = 9, 29, 49$, and with those of the KV model, whose parameters are given by the least-square fits:

$$\begin{cases} \omega_{0,\mathrm{eq}} = \omega_0(1.01 + 0.631\eta_{\mathrm{H}}) \\ \zeta_{\mathrm{V,eq}} = 0.00348 + 0.386\eta_{\mathrm{H}} - 0.296\eta_{\mathrm{H}}^2 \end{cases}; \qquad 0 \leqslant \eta_{\mathrm{H}} \leqslant 0.50$$

It is worth noting that, since the loss modulus of the KV model is linear with frequency (Figure 3(b)), the system damping is underestimated at low frequencies and overestimated at high frequencies.

In Figure 4(a) the cumulative error $e_{|H|}$ on the modulus of the FRF in the interval $[0, 3\omega_0]$ is shown. Only for very low damping are the inaccuracies associated with the LPA and KV models of the same order. Oppositely, for $\eta_{\mathrm{H}} = 0.50$ ($\zeta_{\mathrm{V,eq}} \cong 0.12$) the LPA model with $N_\lambda = 29$ yields an error lower than 3%, while the discrepancies associated with the KV model may be too large for engineering applications, the error being in the order of 13%. As shown

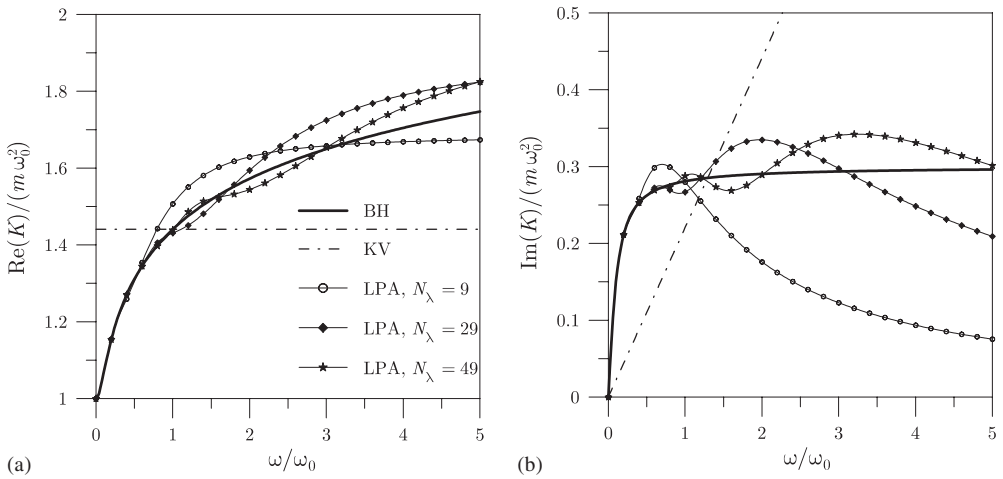

Figure 3. Comparison of: (a) storage moduli; and (b) loss moduli for the Biot hysteretic (BH) and Kelvin–Voigt (KV) models, and for the Laguerre polynomial approximation (LPA).

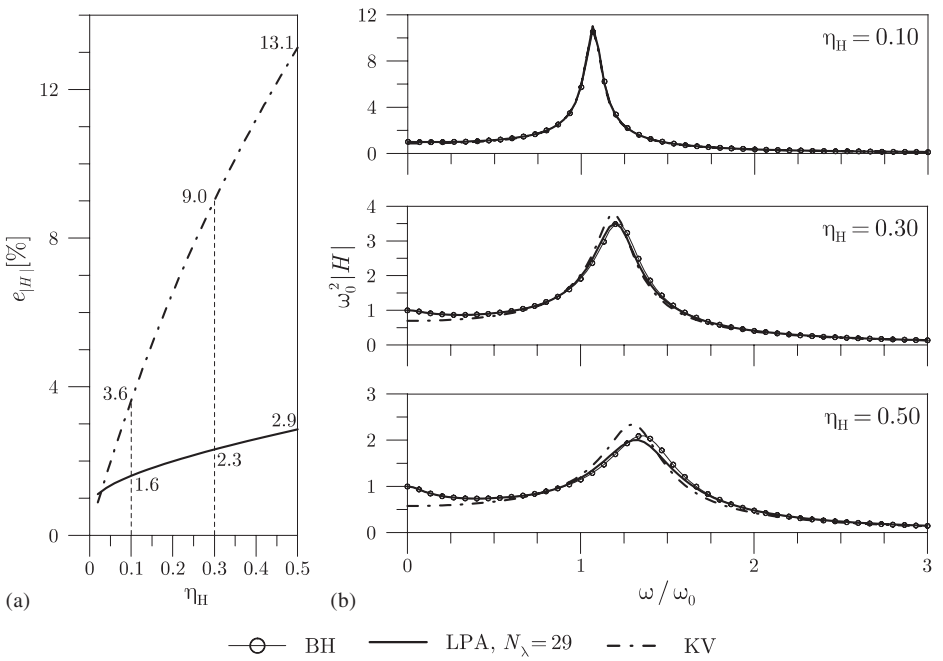

Figure 4. Frequency response functions for the Biot hysteretic (BH) and Kelvin–Voigt (KV) models, and for the Laguerre polynomial approximation (LPA): (a) cumulative errors; and (b) comparison of the absolute values.

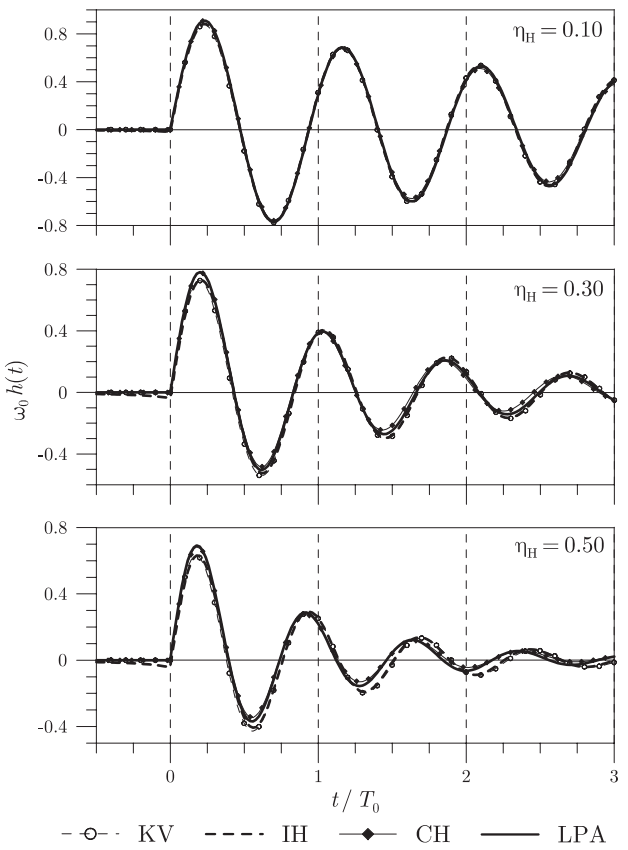

Figure 5. Impulse response function for the Kelvin–Voigt (KV), ideal hysteretic (IH) and causal hysteretic (CH) models, and for the Biot hysteretic model described through the Laguerre polynomial approximation (LPA).

in Figure 4(b), the main differences between the FRFs of the BH and KV models are at low frequencies and at resonance. Note that the FRF $H(\omega)$ of the LPA model can be evaluated as the first element of the complex-valued array:

$$\mathbf{H}(\omega) = (\mathrm{j}\omega\mathbf{I}_{N_\lambda+2} - \mathbf{A})^{-1}\mathbf{b}$$

Finally, the effectiveness of the various models in evaluating the dynamic response of SDoF oscillators with hysteretic damping was examined for three values of the hysteretic loss factor, $\eta_H = 0.10, 0.30, 0.50$. In Figure 5, the impulse response functions $h(t) = \mathscr{F}^{-1}\langle H(\omega)\rangle$ are compared. In Figure 6, the standard deviations $\sigma_X(t)$ of the responses to a stationary Gaussian white noise suddenly applied at $t = 0$, with the oscillator starting from deterministic initial conditions, are also compared. In both cases, the LPA model with $N_\lambda = 29$, previously validated, is used to accurately approximate the responses of the BH model. Figure 5 shows that the differences between the impulse response functions evaluated with the different models increase with η_H, and in particular for $\eta_H = 0.10$ the four lines are almost coincident.

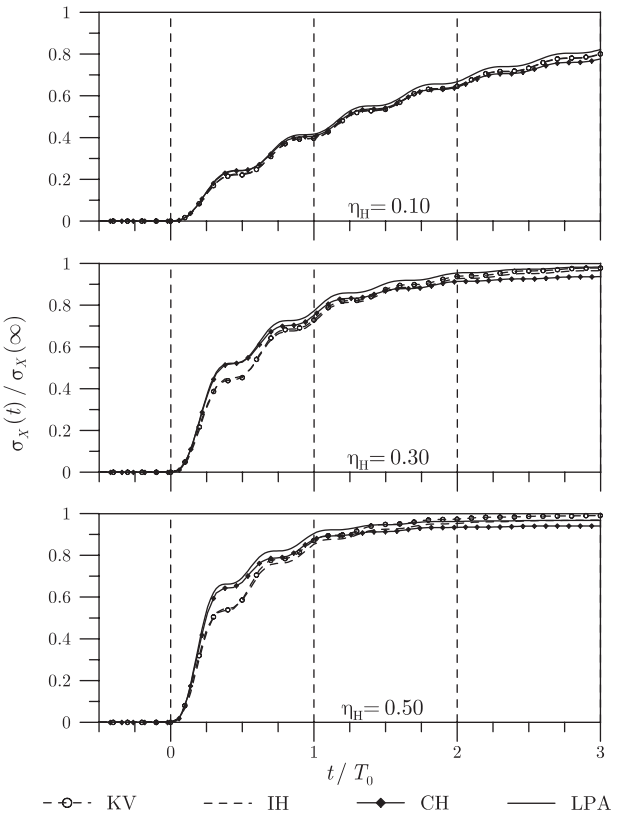

Figure 6. Standard deviation of the non-stationary response of a linear oscillator to white noise for the Kelvin–Voigt (KV), ideal hysteretic (IH) and causal hysteretic (CH) models, and for the Biot hysteretic model described through the Laguerre polynomial approximation (LPA).

Conversely, in Figure 6 differences in the non-stationary standard deviation are not negligible, also for $\eta_H = 0.10$.

5. NUMERICAL EXAMPLE

Within the context of equivalent linear analyses, the BH model proves to be effective in describing the cyclic behaviour of soils [17]. Early experimental research in soil dynamics, in fact, showed that in many cases the dissipative forces experienced in earth structures under small amplitude vibrations are nearly rate independent. In the following, the performance of the proposed procedure will be investigated, through an application to the seismic response of the highway embankment schematically depicted in Figure 7(a) (height $H - h = 18\,\mathrm{m}$; truncation ratio $\ell = h/H = 0.25$). In Figure 7(b) the model used for the stochastic analysis is shown.

Following Dakoulas and Gazetas [24], a shear-beam approximation was used, taking into account the dependence of the soil stiffness on the confining pressure. The average shear modulus (Figure 7(c)) is $G(z) = G_b(z/H)^\mu$, where $G_b = 120\,\mathrm{MPa}$ is the value at the base of

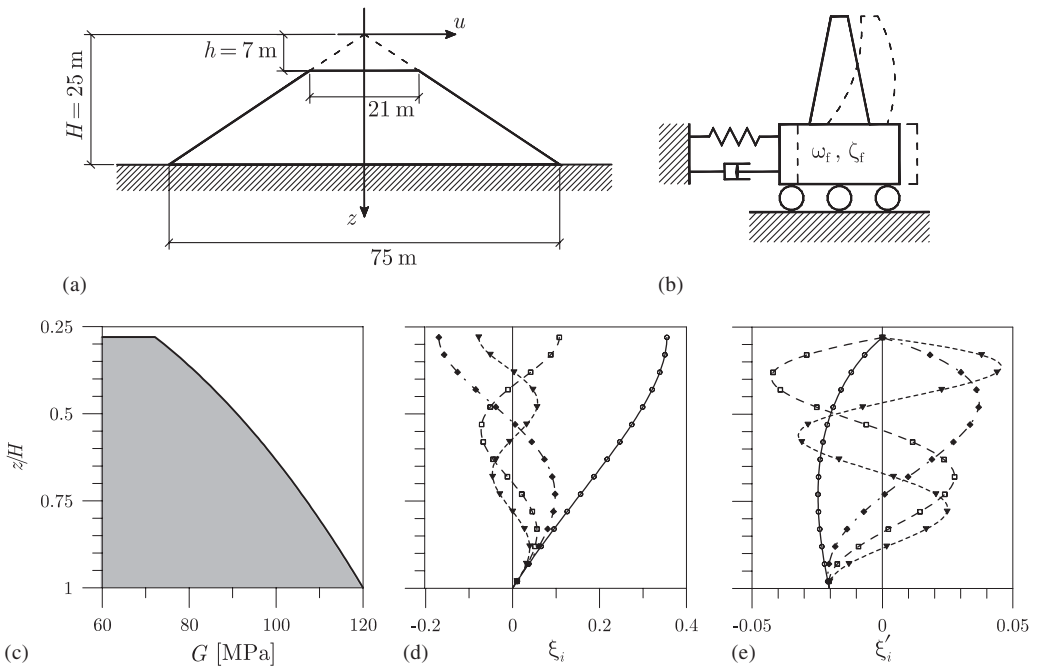

Figure 7. Example embankment: (a) geometry; (b) dynamic model for the stochastic analysis; (c) shear modulus; (d) first modal shapes; and (e) their derivatives.

the embankment, and where $\mu = 0.4$ is the inhomogeneity parameter. The mass density of the soil is $\rho = 2000\,\mathrm{kg/m^3}$, such that the shear wave celerity at the base is $C_\mathrm{b} = \sqrt{G_\mathrm{b}/\rho} \cong 245\,\mathrm{m/s}$. In Figure 7(d) the first four modal shapes $\xi_i(z)$ are depicted, for which the following closed-form expression holds:

$$\xi_i(z) = Y_q(\beta_i) J_q\left[\beta_i \left(\frac{z}{H}\right)^{1-\mu/2}\right] - J_q(\beta_i) Y_q\left[\beta_i \left(\frac{z}{H}\right)^{1-\mu/2}\right]; \quad q = \frac{\mu}{2-\mu}$$

$J_q(\cdot)$ and $Y_q(\cdot)$ being the Bessel functions of the first and second kind, respectively, and where β_i is the i-th non-trivial root of the characteristic equation:

$$Y_q(\beta) J_{q+1}(\beta\lambda^{1-\mu/2}) = J_q(\beta) Y_{q+1}(\beta\lambda^{1-\mu/2}) \tag{26}$$

β_i being related to the i-th natural circular frequency ω_i as:

$$\omega_i = \frac{2-\mu}{2} \beta_i \frac{C_\mathrm{b}}{H}$$

In Figure 7(e), finally, the first derivatives $\xi_i'(z)$ of the modal shapes are depicted. The instantaneous values of the displacement and shear strain over the height of the embankment are:

$$u(z,t) = \sum_i \xi_i(z) y_i(t); \quad \gamma(z,t) = \frac{\partial}{\partial z} u(z,t) = \sum_i \xi_i'(z) y_i(t)$$

$y_i(t)$ being the time history of the i-th modal coordinate.

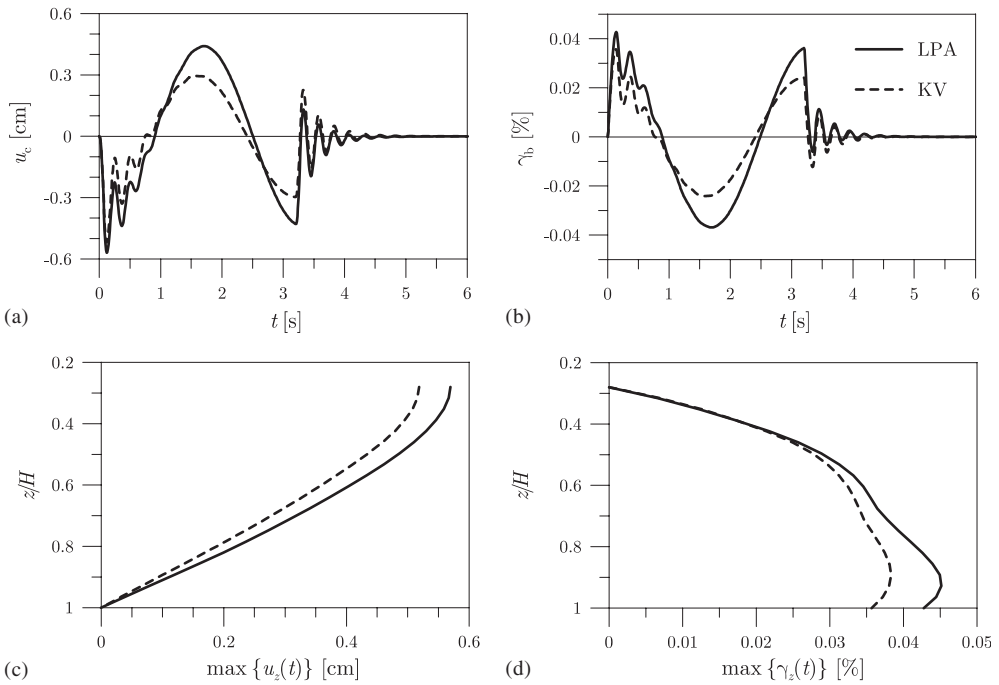

Figure 8. Displacement and shear strains under a deterministic pulse, consistent with the 1979 El Centro earthquake: comparison between the Biot hysteretic model described through the Laguerre polynomial approximation (LPA) and the Kelvin–Voigt (KV) model.

For the example structure, numerical solution of Equation (26) provides the values $\beta_1 = 3.23$, $\beta_2 = 7.75$, $\beta_3 = 12.5$, and $\beta_4 = 17.4$, with a fundamental period $T_1 = 2\pi/\omega_1 = 0.248$ s. The hysteretic loss factor is $\eta_H = 0.44$, corresponding to an equivalent viscous damping ratio $\zeta_{V,eq} \cong 0.12$ in all modes. The motion of the modal oscillators is assumed to be uncoupled, i.e. the structure is proportionally damped.

By using the mode superposition technique, deterministic and stochastic analyses were carried out, in which the response of each mode is governed by Equations (20) and (23), respectively. In a first stage, the deterministic response of the embankment to a simple forward-and-back base motion was evaluated. The excitation was modelled as a one-cosine (type-B) pulse, mathematically expressed as:

$$\ddot{u}_g(t) = \omega_p v_p \cos(\omega_p t)\mathscr{U}(t)\mathscr{U}(T_p - t)$$

where velocity amplitude $v_p = 0.7$ m/s and period $T_p = 2\pi/\omega_p = 3.2$ s are consistent with the fault-normal component of the ground motion recorded during the 1979 El Centro earthquake [25]. The time histories of crest displacement $u_c(t) = u(h,t)$ and of shear strain at the base $\gamma_b(t) = \gamma(H,t)$, evaluated through the Laguerre polynomial approximation (LPA) and Kelvin–Voigt (KV) models, are compared in Figures 8(a) and (b), respectively. The extreme values of displacement and shear strain over the height of the embankment are also compared in Figures 8(c) and (d), respectively. The discrepancies between the results obtained with the

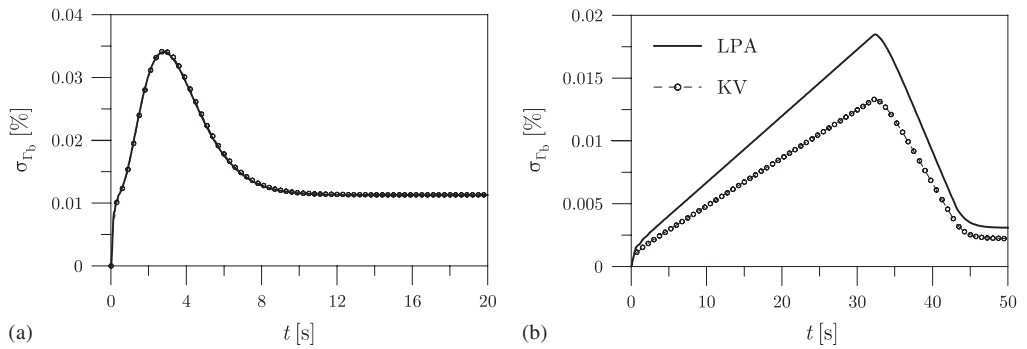

Figure 9. Standard deviation of base shear strain under random excitation consistent with: (a) 1940 El Centro; and (b) 1985 Mexico City earthquakes: comparison between the Biot hysteretic model described through the Laguerre polynomial approximation (LPA) and the Kelvin–Voigt (KV) model.

two models are in the order of 10% for the largest displacement, and of 15% for the largest shear strain.

In a second stage, amplitude modulated outputs of the Kanai–Tajimi filter were used to probabilistically model the frequency and time characteristics of ground accelerations recorded during real earthquakes [26]. For this simple filter, the quantities $\mathbf{A}_\mathrm{f}$, $\mathbf{b}_\mathrm{f}$ and $\mathbf{A}_\mathrm{xf}$ in Equation (22) take the expressions:

$$\mathbf{A}_\mathrm{f} = \begin{bmatrix} 0 & 1 \\ -\omega_\mathrm{f}^2 & -2\zeta_\mathrm{f}\omega_\mathrm{f} \end{bmatrix}; \quad \mathbf{b}_\mathrm{f} = \begin{bmatrix} 0 \\ 1 \end{bmatrix}; \quad \mathbf{A}_\mathrm{xf} = \begin{bmatrix} 0 & 0 \\ -\omega_\mathrm{f}^2 & -2\zeta_\mathrm{f}\omega_\mathrm{f} \end{bmatrix}$$

For the 1940 El Centro earthquake, the circular frequency (accounting for the central frequency of the acceleration) is $\omega_\mathrm{f} = 19.0\,\mathrm{rad/s}$, the damping ratio (controlling the spread of the frequency content) is $\zeta_\mathrm{f} = 0.45$, and the power spectral density of the forcing white noise (related to the total energy of the earthquake) is $S_W = 0.014\,\mathrm{m^2/s^{-3}}$; in addition, the amplitude of the excitation is modulated through the smooth function:

$$\varphi(t) = \varphi_\infty + (1 - \varphi_\infty)\left(\frac{t}{t_\mathrm{p}}\right)^3 \exp\left[3\left(1 - \frac{t}{t_\mathrm{p}}\right)\right], \quad t \geqslant 0$$

with $t_\mathrm{p} = 2.6\,\mathrm{s}$ and $\varphi_\infty = 0.33$. For the 1985 Mexico City earthquake the selected values are $\omega_\mathrm{f} = 1.1\pi\,\mathrm{rad/s}$, $\zeta_\mathrm{f} = 0.12$, and $S_W = 0.020\,\mathrm{m^2/s^{-3}}$, while the amplitude modulating function is piecewise linear:

$$\varphi(t) = \begin{cases} 0.104 + 0.0280t, & 0 \leqslant t < t_1 = 32.0\,\mathrm{s} \\ 1 - 0.0768(t - t_1), & t_1 \leqslant t < t_2 = 42.9\,\mathrm{s} \\ 0.163, & t \geqslant t_2 \end{cases}$$

In Figure 9 the standard deviations of the non-stationary random process $\Gamma_\mathrm{b}(t)$ describing the base shear strain are compared, as evaluated with LPA and KV models. Depending on the spectral characteristics of the ground motion, the KV approximation brings accurate estimation

(Figure 9(a)) or unacceptable errors (Figure 9(b)). In particular, in the case of the Mexico City earthquake the inaccuracy associated with the KV model is of about 28%.

6. CONCLUSIONS

In this paper, the most common models for the analysis of dynamic systems featuring linear hysteretic damping have been compared and criticised. The ideal hysteretic model, though of simple use in the frequency domain, is inconsistent when used in the time domain, as it does not satisfy the causality requirement. The causal hysteretic model, constructed to overcome the non-causality flaw, is pathological, due to a singularity at the static limit. Finally, the viscoelastic Biot hysteretic model proves to be the simplest, causal and physically realizable model in representing the dynamic behaviour of systems with rate-independent energy dissipation, but its practical use requires the solution of integrodifferential equations.

In order to overcome this difficulty, a particularization of the Laguerre polynomial approximation (LPA) method has been proposed, which allows turning the integrodifferential equations of motion into a set of differential equations, whose solution is not excessively time consuming. Oppositely to alternative approximations of the Biot hysteretic model recently published, closed-form expressions have been derived for the parameters of the proposed approximation. Moreover, very efficient step-by-step solution schemes for both deterministic and random excitations have been provided. The convergence rate and the associated error have been also investigated in the frequency domain, showing that the LPA method is very accurate, even for high levels of damping.

Finally, the proposed approach has been validated through the application to the vibration analysis of a highway embankment excited by deterministic and random ground motions, consistent with recorded earthquakes. The response evaluated by using the LPA method has been compared with the response of an equivalent viscous system, and the inaccuracy associated with this approximation was found to be in some cases unacceptable for engineering purposes.

REFERENCES

1. Myklestad NO. The concept of complex damping. *Journal of Applied Mechanics* 1952; **19**:284–286.
2. Bishop RED. The treatment of damping forces in vibration theory. *Journal of the Royal Aeronautical Society* 1955; **59**:738–742.
3. Reid TJ. Free vibration and hysteric damping. *Journal of the Royal Aeronautical Society* 1956; **60**:283.
4. Lancaster P. Free vibration and hysteric damping. *Journal of the Royal Aeronautical Society* 1960; **64**:229.
5. Caughey TK. Vibration of dynamic systems with linear hysteretic damping (linear theory). *Proceedings of the 4th US National Congress of Applied Mechanics*, *ASCE*, 1962, Berkeley, U.S.A., **1**:87–97.
6. Crandall SH. The role of damping in vibration theory. *Journal of Sound and Vibration* 1970; **11**(1):3–18.
7. Gaul L, Bohlen S, Kempfle S. Transient and forced oscillations of systems with constant hysteretic damping. *Mechanics Research Communications* 1985; **12**(4):187–201.
8. Milne HK. The impulse response function of a single degree of freedom system with hysteretic damping. *Journal of Sound and Vibration* 1985; **100**(4):590–593.
9. Inaudi JA, Kelly JM. Linear hysteretic damping and the Hilbert transform. *Journal of Engineering Mechanics* (ASCE) 1995; **121**(5):626–632.
10. Chen JT, You DW. Hysteretic damping revisited. *Advances in Engineering Software* 1997; **28**:165–171.
11. Chen JT, You DW. An integral-differential equation approach for the free vibration of a SDoF system with hysteretic damping. *Advances in Engineering Software* 1999; **30**:43–48.
12. Inaudi JA, Makris N. Time-domain analysis of linear hysteretic damping. *Earthquake Engineering and Structural Dynamics* 1996; **25**:529–545.
13. Inaudi JA. Analysis of hysteretic damping using analytical signals. *Journal of Engineering Mechanics* (ASCE) 1997; **123**(7):743–745.

14. Makris N. Stiffness, flexibility, impedance, mobility and hidden delta function. *Journal of Engineering Mechanics* (ASCE) 1997; **123**(11):1202–1208.
15. Makris N. Causal hysteretic element. *Journal of Engineering Mechanics* (ASCE) 1997; **123**(11):1209–1214.
16. Biot MA. Linear thermodynamics and the mechanics of solids. *Proceedings of the 3rd US National Congress of Applied Mechanics*, *ASCE*, 1958, Providence, U.S.A., 1–18.
17. Makris N, Zhang J. Time domain viscoelastic analysis of earth structures. *Earthquake Engineering and Structural Dynamics* 2000; **29**:745–768.
18. Spanos PD, Tsavachidis S. Deterministic and stochastic analyses of a nonlinear system with a Biot visco-elastic element. *Earthquake Engineering and Structural Dynamics* 2001; **30**:595–612.
19. Spanos PD, Zeldin BA. Pitfalls of deterministic and random analyses of systems with hysteresis. *Journal of Engineering Mechanics* (ASCE) 2000; **126**(10):1108–1110.
20. Palmeri A, Ricciardelli F, De Luca A, Muscolino G. State space formulation for linear viscoelastic dynamic systems with memory. *Journal of Engineering Mechanics* (ASCE) 2003; **129**(7):715–724.
21. Palmeri A, Ricciardelli F, Muscolino G, De Luca A. Effects of viscoelastic memory on the buffeting response of tall buildings. *Wind and Structures* 2004; **7**(2):89–106.
22. Palmeri A, Ricciardelli F, Muscolino G, De Luca A. Random vibration of systems with viscoelastic memory. *Journal of Engineering Mechanics* (ASCE) 2004; **130**(9):1052–1061.
23. Muscolino G. Dynamically modified linear structures: deterministic and stochastic response. *Journal of Engineering Mechanics* (ASCE) 1996; **122**(11):1044–1051.
24. Dakoulas P, Gazetas G. A class of inhomogeneous shear models for seismic response of dams and embankments. *Soil Dynamics and Earthquake Engineering* 1985; **4**(4):166–182.
25. Makris N. Rigidity–plasticity–viscosity: can electrorheological dampers protect base-isolated structures from near-source ground motions? *Earthquake Engineering and Structural Dynamics* 1997; **26**:571–591.
26. Fan FG, Ahmadi G. Nonstationarity Kanai–Tajimi models for El Centro 1940 and Mexico City 1985 earthquakes. *Probabilistic Engineering Mechanics* 1990; **5**(4):171–181.

